

Perovskite Solar Cells

How to cite: *Angew. Chem. Int. Ed.* **2020**, *59*, 15688–15694

International Edition: doi.org/10.1002/anie.202005211

German Edition: doi.org/10.1002/ange.202005211

Stabilization of Highly Efficient and Stable Phase-Pure FAPbI₃ Perovskite Solar Cells by Molecularly Tailored 2D-OverlayersYuhang Liu⁺,* Seckin Akin⁺, Alexander Hinderhofer, Felix T. Eickemeyer, Hongwei Zhu, Ji-Youn Seo, Jiahuan Zhang, Frank Schreiber, Hong Zhang, Shaik M. Zakeeruddin, Anders Hagfeldt, M. Ibrahim Dar,* and Michael Grätzel*

Abstract: As a result of their attractive optoelectronic properties, metal halide APbI₃ perovskites employing formamidinium (FA⁺) as the A cation are the focus of research. The superior chemical and thermal stability of FA⁺ cations makes α -FAPbI₃ more suitable for solar-cell applications than methylammonium lead iodide (MAPbI₃). However, its spontaneous conversion into the yellow non-perovskite phase (δ -FAPbI₃) under ambient conditions poses a serious challenge for practical applications. Herein, we report on the stabilization of the desired α -FAPbI₃ perovskite phase by protecting it with a two-dimensional (2D) IBA₂FAPb₂I₇ (IBA = iso-butylammonium overlayer, formed via stepwise annealing. The α -FAPbI₃/IBA₂FAPb₂I₇ based perovskite solar cell (PSC) reached a high power conversion efficiency (PCE) of close to 23%. In addition, it showed excellent operational stability, retaining around 85% of its initial efficiency under severe combined heat and light stress, that is, simultaneous exposure with maximum power tracking to full simulated sunlight at 80°C over 500 h.

Introduction

Owing to their high power conversion efficiency (PCE) exceeding 25% and ease of production, hybrid organic metal halide perovskite solar cells (PSCs) are presently attracting wide attention both from the scientific community and photovoltaic industry.^[1–8] Most PSCs employ formulations containing methylammonium (MA⁺) cations which however are unstable decomposing to methylamine upon exposure to heat, moisture, and light.^[9–14] Therefore, for the large-scale deployment of highly-efficient PSCs, the intrinsic instability issues associated with the loss of MA⁺ cations need to be mitigated.^[7,15–21] In this regard, the formamidinium (FA⁺) cation offers an attractive alternative to MA⁺ as pristine FAPbI₃ features lower volatility and close to optimal Goldschmidt tolerance factor,^[22] as well as an absorption edge extending into the near IR to around 840 nm, rendering pristine FAPbI₃ a more efficient solar light than MAPbI₃.^[4,23–25] However, the spontaneous formation of the photo-voltaically inactive, non-perovskite yellow phase (δ -FAPbI₃) below the α to δ phase transition at 170°C^[17,26] causes a serious predicament, introducing Cs⁺, or MA⁺ into the FAPbI₃ lattice prevents the formation of its delta phase, However, the incorporation of these ions affects the spectral response and operational stability of the resulting PSCs under heat stress and in humid conditions.^[4,27–29]

Herein we achieve stabilization of the α -FAPbI₃ phase by introducing a stepwise annealing process and covering it with a novel two-dimensional IBA₂FAPb₂I₇ ($n=2$) perovskite layer containing iso-butylammonium (IBA) as a spacer layer. The confluence of stepwise annealing and IBA₂FAPb₂I₇ lamination allowed the formation of pristine α -FAPbI₃ films containing long-lasting charge-carriers with lifetime exceeding 1.5 μ s. These desired structural and spectral features translated into high photovoltage of 1113 mV as compared to 1053 mV for reference, leading to the realization of a PCE close to 23%, one of a record for FAPbI₃-based PSCs. Remarkably we achieved excellent operational stability, the PSCs retaining around 95% of their initial efficiency at the maximum power point (MPP) under full-sun illumination over 700 h. The superior robustness of the FAPbI₃ protected by the 2D overlayer was further confirmed by long term testing under harsh simultaneous heat and light stress. These devices showed only small degradation under full-sun illumination for 500 hours at 80°C, while unprotected FAPbI₃ films lost rapidly over 60% of their initial performance.

[*] Dr. Y. Liu,^[†] Dr. S. Akin,^[†] Dr. F. T. Eickemeyer, H. Zhu, Dr. J.-Y. Seo, Dr. H. Zhang, Dr. S. M. Zakeeruddin, Dr. M. I. Dar, Prof. M. Grätzel
Laboratory of Photonics and Interfaces
Department of Chemistry and Chemical Engineering
École Polytechnique Fédérale de Lausanne
1015 Lausanne (Switzerland)
E-mail: yuhang.liu@epfl.ch
ibrahim.dar@epfl.ch
michael.gratzel@epfl.ch

Dr. A. Hinderhofer, Prof. F. Schreiber
Institut für Angewandte Physik, Universität Tübingen
72076 Tübingen (Germany)

J. Zhang, Prof. A. Hagfeldt
Laboratory of Photomolecular Science
École Polytechnique Fédérale de Lausanne
Station 6, 1015 Lausanne (Switzerland)

Dr. S. Akin^[†]
Department of Metallurgical and Materials Engineering
Karamanoglu Mehmetbey University
Karaman (Turkey)

[†] These authors contributed equally to the work.

Supporting information and the ORCID identification number(s) for the author(s) of this article can be found under:
https://doi.org/10.1002/anie.202005211.

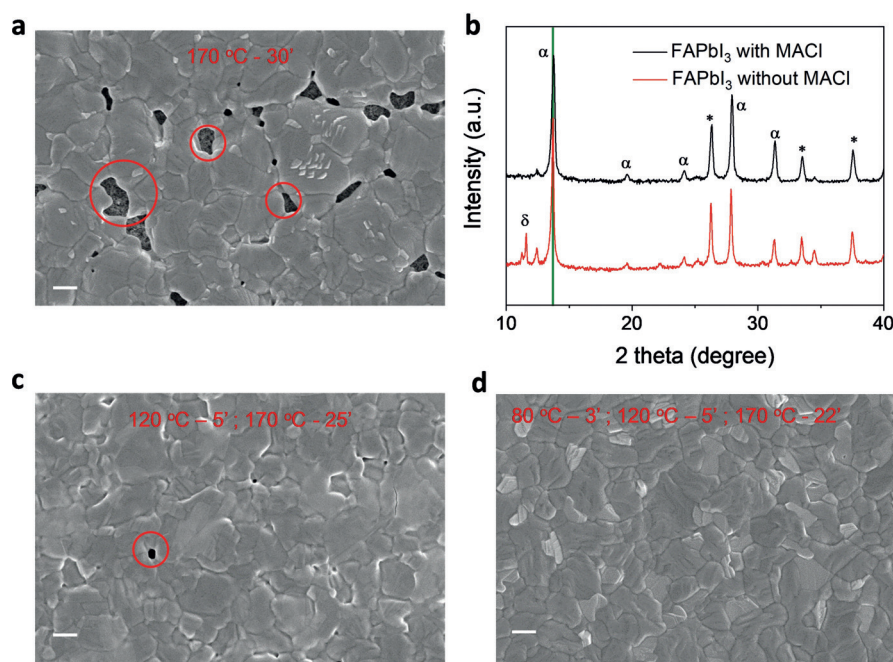


Figure 1. a) Morphological and structural analysis: Single-step annealing treatment, b) XRD patterns of FAPbI₃ perovskite with and without MACI treatment. c) two-step annealing treatment and d) three-step annealing treatment. Representative pinholes are highlighted in red circle, and the scale bars represent 500 nm in length.

Results and Discussion

Stepwise annealing for high-quality FAPbI₃ perovskite film

We employed methylammonium chloride (MACI)^[30] as a crystallization aid to form films of pure α -FAPbI₃ containing only trace amounts of yellow δ -FAPbI₃ phase as established by grazing incidence wide angle synchrotron X-ray diffraction (GIWAX), and absorption and photoluminescence analysis.^[30] Details are presented in Supporting Information Note 1 and Figures S2–S5. Top-view scanning electron microscopy (SEM) pictures of the FAPbI₃ perovskite films with and without MACI treatment are shown in Figure 1a and Figure S1, respectively and reveal that the MACI treatment reduces their surface roughness. To probe the formation of δ -FAPbI₃ phase, X-ray diffraction (XRD) patterns were recorded, and the results are shown in Figure 1b. The FAPbI₃ films formed in the absence of MACI exhibit a peak at $2\theta = 11.6^\circ$, resulting from the presence of δ -phase. By contrast, MACI-treated FAPbI₃ sample shows a weak feature, indexable to PbI₂. However, the formation of large pinholes is apparent presumably related to the rapid release of gaseous MACI. Such pinholes mostly cause shunts resulting in low PCEs (Figure S6) and poor stability. To prevent their formation we applied a stepwise annealing procedure as shown in Figure S7. An intermediate annealing step at 120 °C for 5 min substantially reduced the amount of pin holes in the FAPbI₃ perovskite film as shown in Figure 1c. Finally, we obtained smooth and conformal FAPbI₃ perovskite films composed of micron-sized grains as shown in Figure 1d by optimizing a three-step annealing procedure.

Power conversion efficiencies (PCE) obtained with such films using the FTO/TiO₂/perovskite/spiro-OMeTAD/Au architecture are shown in Table 2. We achieved a maximum PCE of approximately 20.4% with such MACI-treated and stepwise annealed FAPbI₃ perovskite films. In contrast, PSCs made without the stepwise annealing procedure yielded a PCE of only 15.5% (Figure S6) due to a significantly lower open circuit voltage (V_{OC}) and fill factor (FF) ascribed to the poor film quality.

Surface treatment and structural characterization of FAPbI₃-based perovskite

Although the as-prepared FAPbI₃ perovskite films were phase pure (See Supporting Information, note 1) and yielded PCEs of up to 20.4%, prolonged exposure to ambient air led to the formation of photo-inactive phases, that is, PbI₂ and δ -FAPbI₃ as shown in Figure S8. To avoid this degradation and further improve the PCE, we introduced iso-butylammonium iodide (IBAI) as to form a 2D-protective layer on top of the 3D α -FAPbI₃ phase (Figure 2a). Our treatment involved spin-coating a 30 mM solution of IBAI in isopropanol on the surface of as-prepared FAPbI₃ perovskite films followed by annealing at 110 °C for 10 min. We ascertained by SEM that this treatment did not alter the morphology of the underneath photoactive layer (Figure S9).

We investigated the structure of the overlayer formed by the IBA surface treatment using grazing incidence wide-angle X-ray scattering (GIWAXS) and present data in Figure 2b. The GIWAXS reflections show distinct diffraction patterns, which we indexed to the structure of the 2D-perovskite

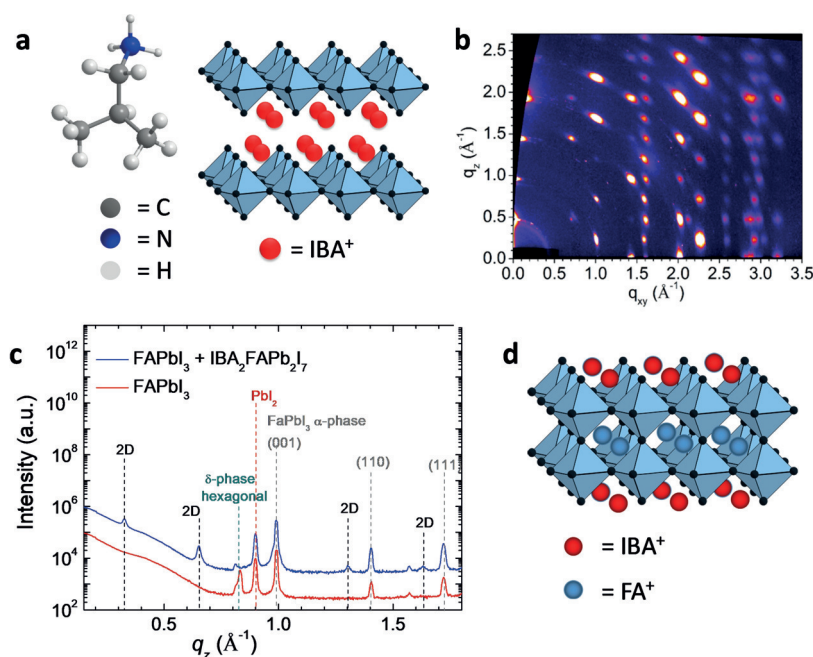


Figure 2. a) Chemical structure of IBA⁺ and schematic illustration of pure 2D-IBA₂PbI₄ perovskite. b) GIWAXS data of pure 2D-IBA₂PbI₄ (angle of incidence = 0.14°). c) X-ray reflectivity data of a bare FAPbI₃ film, and FAPbI₃/2D-IBA₂FAPb₂I₇ prepared by the stepwise annealing method. d) a schematic illustration of pure 2D-IBA₂FAPb₂I₇ perovskite.

IBA₂PbI₄. Table 1. summarizes the orthorhombic unit cell dimensions derived from fitting the GIWAXS data. For comparison, we show also the unit cell parameters of the previously reported structural analogous butylammonium lead iodide (BA₂PbI₄).^[31] Compared to the BA₂PbI₄, the unit cell of IBA₂PbI₄ is smaller, mainly because the long unit cell axis is shortened by 1.5 Å, which is consistent with the alkyl chain length difference in the two organic spacer molecules.

X-ray reflectivity (XRR) data of pristine and IBAI treated FAPbI₃ films are shown in Figure 2c. Each film exhibits structural features corresponding to the α-FAPbI₃ perovskite phase with a lattice spacing of 6.36 Å,^[32] the hexagonal FAPbI₃ (non-perovskite phase)^[33] and PbI₂. The IBAI treated FAPbI₃ films revealed the formation of IBA₂FAPb₂I₇ overlayer exhibiting reflections of the 2D-structure with a lattice spacing of 38.56 Å. The lattice spacing is slightly smaller than the lattice spacing of the BA₂FAPb₂I₇ (*n* = 2) structure of 39.35 Å,^[34] which is consistent with the length difference in the spacer molecules BAI and IBAI. To our knowledge, this is the first investigation of iso-butyl as a spacer layer in perovskites for PSCs. Cho et al.^[35] used mixtures of n-butyl and iso-butylammonium cations for surface passivation treatments yielding a PCE of 21.7% mixed cation.

Table 1: Unit cell parameters of BA₂PbI₄^[31] and IBA₂PbI₄ based 2D perovskites.

2D Perovskite	<i>a</i>	<i>b</i>	<i>c</i>	<i>V</i>
2D-BA ₂ PbI ₄	8.87	8.69	27.6	2129
2D-IBA ₂ PbI ₄	8.9	8.7	26.2	2029

GIWAXS data of pristine and IBAI treated FAPbI₃ films (Figure 3a, b) confirm the formation of α-FAPbI₃ perovskite-phase in agreement with the XRR measurements. The additional 2D reflections (Figure 3b) arising from the 2D-IBA₂FAPb₂I₇ overlayer are along the q_z axis indicating their orientation to be parallel to the substrate. With the radially integrated data over the measured *q*-space, (Figure 3c) we can qualitatively estimate the amount of PbI₂ and hexagonal phase FAPbI₃ in the scattering volume. In the sample with 2D-IBA₂FAPb₂I₇ overlayer, a negligible content of the hexagonal polymorph and a smaller amount of excess PbI₂ compared to the non-covered sample is observed. This establishes that FA from the δ-FAPbI₃ structure is consumed in the formation of the IBA₂FAPb₂I₇ layer. As compared to IBA₂PbI₄ (*n* = 1) system, IBA₂FAPb₂I₇ passivating layer, a tailored 2D system, should demonstrate better charge transport while concurrently rendering the resulting PSC less susceptible to the moisture uptake.

Charge-carrier dynamics

We further investigated the impact of the IBA₂FAPb₂I₇ layer on the optoelectronic properties of the α-FAPbI₃ perovskite films using time-resolved photoluminescence (TRPL) as shown in Figure 3d. Both the untreated and treated films show two distinct decay regimes. A very fast decay within the first 10 ns is followed by a slow mono-exponential decay. The fast decay at early times is caused by carrier diffusion due to the initial exponential excitation profile in combination with charge carrier trapping very likely caused by shallow traps on or near the surface (PbI₂, δ-FAPbI₃ non-perovskite phase or surface states). The IBAI

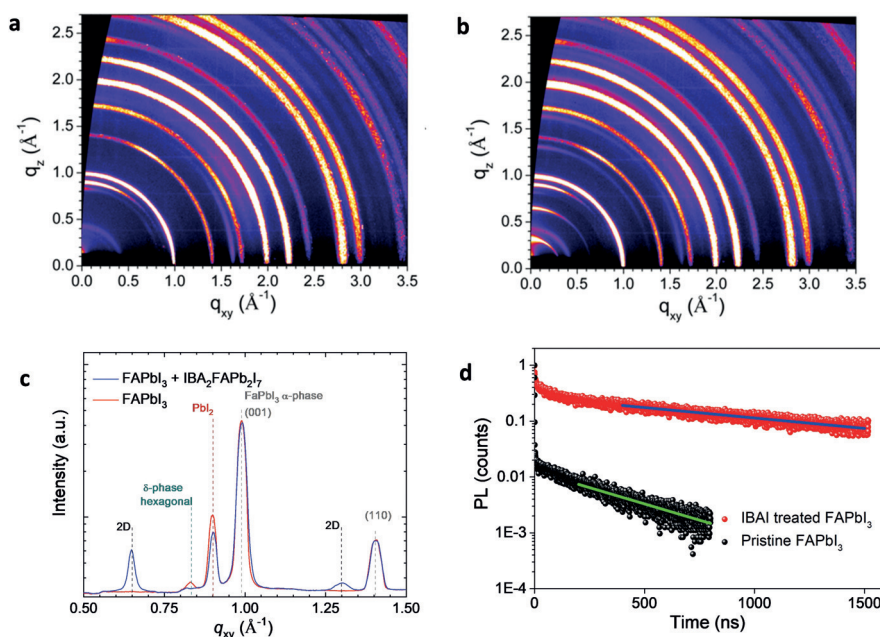


Figure 3. Structural and spectroscopic characterization. GIWAXS data of a) FAPbI₃ film b) FAPbI₃/2D IBA₂FAPb₂I₇. Angle of incidence was 0.14°. c) Radially integrated GIWAXS data from (a,b). d) TRPL results of neat FAPbI₃, and FAPbI₃/IBA₂FAPb₂I₇-based perovskites. The blue and green curves are fits to the kinetic model published previously.^[34] Both cases ($k=0$ and $S=0$ for FBAI treated films) result in the same fit.

treated film shows a slower decay by more than one order of magnitude within the first 10 ns compared to the untreated film. Since the carrier diffusion rate is the same in both films, we infer that the IBAI treatment alters the defect chemistry of the surface which leads to a significantly lower trap density. Also the first-order decay kinetics at times > 10 ns are much slower for the treated than the untreated films. We applied numerical simulations to analyze the different decay kinetics. Details for this simulation can be found in Zhu et al.^[36] The single exponential decay can be caused by either SRH recombination with a recombination constant k_1 or by surface recombinations with a surface recombination velocity S . Since both films have the same bulk material and, hence, the same k_1 , the only difference lies in S . We considered two extreme cases for the IBAI treated film, where in the first case the film exhibits no bulk recombinations ($k_1=0$), that is, the mono-exponential decay is exclusively caused by surface recombination. Conversely, in the second case, we assume that the film exhibits no surface recombination ($S=0$), that is, the decay is solely caused by SRH type bulk recombination. From this, we calculated the difference in velocity of surface recombination for the two films to be $\Delta S = 32 \text{ cm s}^{-1}$ which is the same in both extreme cases. The details of this calculation can be found in Table S1 and the fitted curves are shown in Figure 3d. This shows that IBAI treatment not only reduces the level of PbI₂ and δ -FAPbI₃ near the surface but it also efficiently passivates electronic trap states likely caused by these impurities at or near the surface of the perovskite film. This improvement in the optoelectronic film quality has an impact on the device performance and in particular in the V_{oc} as will be shown in the following.

Photovoltaic performance and operational stability

To investigate the potential impact of combining the stepwise annealing with the introduction of a 2D-IBA₂FAPb₂I₇ layer on the photovoltaic performance we fabricated PSCs of the architecture FTO/compact-TiO₂/mesoscopic-TiO₂/perovskite/2D-layer/spiro-OMeTAD/gold (Figure S10). Representative $J-V$ curves of PSCs with and without 2D IBA₂FAPb₂I₇ perovskite layer are shown in Figure 4a, from which we deduce the photovoltaic metrics summarized in Table 2. The device using neat FAPbI₃ subjected to treatment with MAI and stepwise sintering, showed a PCE of 20.4% with a V_{oc} of 1053 mV, a J_{sc} of 25.87 mA cm^{-2} and a fill factor of 77.2%. Covering the perovskite film with the 2D-IBA₂FAPb₂I₇ layer enhances substantially all three PV metrics, the champion PSC achieving a PCE of 22.7%, with $V_{oc}=1113 \text{ mV}$, $J_{sc}=25.83 \text{ mA cm}^{-2}$ and FF = 80.5%, which is one of the best efficiency values reported for all-iodide FAPbI₃-based PSCs. We attribute the increase in the V_{oc} , that is, $\Delta V_{oc} = 191 \text{ mV}$ and 59 mV with regards to bare FAPbI₃ films, with and without stepwise annealing, respectively, as well as the outstanding FF of 80.5% to the effective suppression of δ -FAPbI₃ phase formation together with the surface trap mitigation effect of the IBA₂FAPb₂I₇ overlayer. The surface treatment of the FAPbI₃ perovskite with IBAI converts most of the δ -FAPbI₃ into the 2D IBA₂FAPb₂I₇ surface layer, any residue being below the detection limit of our GIWAXS measurements. The removal of δ -FAPbI₃ prolongs the charge carrier lifetime as revealed by the TRPL measurements, enabling the high V_{oc} values observed for PSCs that are endowed with an α -FAPbI₃/IBA₂FAPb₂I₇ overlayer.^[37] In addition, the photovoltaic performance of *n*-butyl ammonium

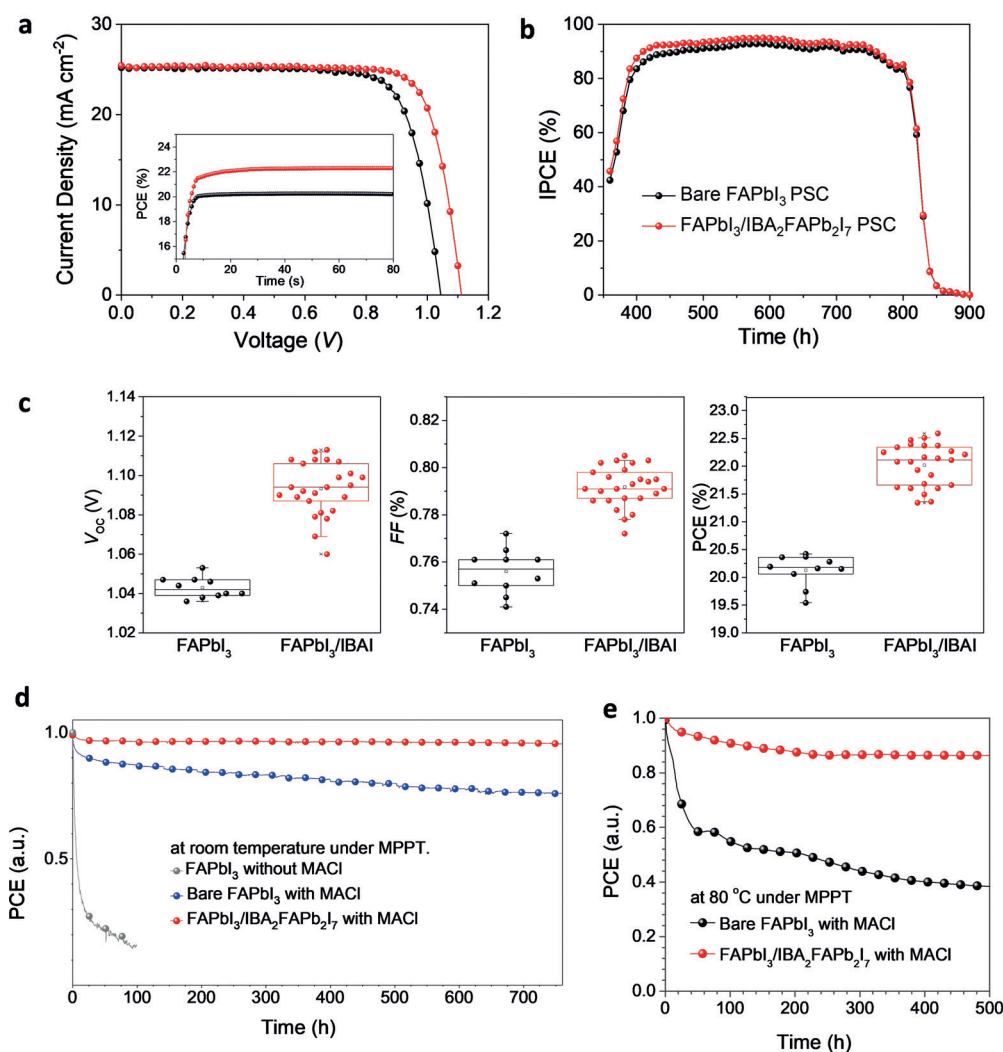


Figure 4. Photovoltaic and stability measurements: a) $J-V$ curves, b) IPCE curves, c) V_{OC} , FF, and PCE matrix, d) and e) ageing results of PSCs based on bare FAPb₃ (black or blue dotted line) α -FAPb₃/IBA₂FAPb₂I₇ perovskites (red dotted line). The inset of (a) shows the MPP tracking data of PSCs based on bare FAPb₃ and α -FAPb₃/IBA₂FAPb₂I₇ perovskites.

iodide (BAI) surface treated FAPb₃ based perovskite is summarized in Figure S11. Champion cell with BAI treatment yielded PCE up to 21.8%, as compared to 22.7% with IBAI treatment and 20.4% untreated. The statistic results prove superior photovoltaic performance of IBAI treated PSC as compared to BAI.

The inset of Figure 4a shows the tracking of the maximum power point (MPPT) for two cells with and without 2D-overlayer over the first 60 seconds. The power output (SPO) of the device endowed with the 2D layer reached a stabilized

Table 2: Photovoltaic parameters of PSCs based on stepwise annealing FAPb₃ and FAPb₃/IBAI (measured under simulated AM 1.5G solar irradiance at 100 mWcm⁻²).^[a]

Device	V_{OC} [mV]	J_{SC} [mAcm ⁻²]	FF [%]	PCE [%]
FAPb ₃	1053 (1043)	25.87 (25.41)	77.2 (75.6)	20.4(20.1)
FAPb ₃ /IBAI	1113 (1093)	25.83 (25.36)	80.5 (79.2)	22.7(22.1)

[a] The values in parentheses are the average values of 10 PSC devices for FAPb₃, and 25 PSC devices for α -FAPb₃/IBA₂FAPb₂I₇.

value of around 22.4%. within 10 s This yields an SPO-to-PCE ratio of 0.99, implying a reliable solar energy output.^[38] Statistics of photovoltaic parameters corresponding to IBA₂FAPb₂I₇ layer-based PSCs are summarized and compared with those obtained for 2D-layer free PSCs in Figure 4c. Enhanced V_{OC} , FF, and PCE values were obtained for over 25 perovskite devices endowed IBA₂FAPb₂I₇ overlayers, further revealing the effectiveness of using the 2D layer for passivating defects and for improving the photovoltaic performance.

Figure 4b shows incident photon to electron conversion efficiency (IPCE) spectra of PSCs with and without IBA₂FAPb₂I₇ surface treatment layer. The integrated photocurrents are in excellent agreement with $J-V$ measurements, their difference being under 2%. To evaluate the effects of the film treatment on the long-term device stability, we record the operational stability of the PSCs by exposing unsealed devices at room temperature to full-sun illumination in flowing nitrogen gas while tracking their MPP (Figure 4d). After 700 h, FAPb₃ PSC endowed with the 2D IBA₂FAPb₂I₇

layer retained over 95% of its initial efficiency, proving excellent operational stability. In comparison, MAI treated PSCs without IBA₂FAPb₂I₇ surface layer retained merely 76% of their initial efficiency. To further substantiate the superior operational stability of FAPbI₃-based PSCs, we also performed MPP tracking experiment under simulated full-sun irradiance at 80°C for FAPbI₃-based PSC with and without 2D IBA₂FAPb₂I₇ layer (Figure 4e). After over 500 h, the cell using a 2D IBA₂FAPb₂I₇ overlayer retained 84% of its initial efficiency while the PCE of the bare FAPbI₃ dropped to less than 26%. The robust performance of α -FAPbI₃/IBA₂FAPb₂I₇-based PSCs results from the suppression of the δ -FAPbI₃ phase, better perovskite film quality, and superior moisture stability of α -FAPbI₃/IBA₂FAPb₂I₇ layer (Figure S12).^[38–40] FAPbI₃ films produced without the stepwise annealing and MAI treatment degrade severely within the first few hours of aging. Thus the new results obtained in our study set new benchmarks in terms of both efficiency and stability for FAPbI₃-based PSCs.

Conclusion

In conclusion, using a stepwise annealing method, FAPbI₃-based perovskites have been stabilized by effectively suppressing the formation of the δ -FAPbI₃ non-perovskite phase. By exploiting the catalytic activity of MAI together with a surface coating of a molecularly tailored IBA₂FAPb₂I₇ layer, a PCE approaching 23% was achieved, which is amongst the highest values reported for pure FAPbI₃-based PSCs. Such 2D coated PSCs exhibited superior operational stability under a heat stress of 80°C. Our work provides an efficient and cost-effective way to stabilize and to improve the operational stability of FAPbI₃-based perovskite, paving the way for the industrialization of PSCs.

Acknowledgements

Y.L. S.M.Z., and M.G. thank the King Abdulaziz City for Science and Technology (KACST) and the European Union's Horizon 2020 research and innovation program under grant agreement No 826013 for financial support. A.H. thanks the financial support from the European Union's Horizon 2020 research and innovation programme under grant agreement No 764047. H.Z. thanks the China Scholarship Council for financial support. A.H. acknowledges the financial support from the Swiss National Science Foundation R'Equip program under the grant number 183305. We thank Mr. Aditya Mishra, Dr. Michael Hope and Prof. Lyndon Emsley from EPFL for their help on solid-state NMR research. M.I.D. acknowledges the financial support from the Swiss National Science Foundation (SNSF) under project number P300P2_174471. We acknowledge the European Synchrotron Radiation Facility (ESRF) for provision of synchrotron radiation facilities and we would like to thank Oleg Kononov for assistance in using beamline ID10.

Conflict of interest

The authors declare no conflict of interest.

Keywords: additive engineering · FAPbI₃ · perovskite solar cells · thermal stability

- [1] NREL, Best research efficiencies: <https://www.nrel.gov/pv/assets/pdfs/best-research-cell-efficiencies.20200406.pdf>.
- [2] A. Kojima, K. Teshima, Y. Shirai, T. Miyasaka, *J. Am. Chem. Soc.* **2009**, *131*, 6050–6051.
- [3] D. Bi, C. Yi, J. Luo, J.-D. Décoppet, F. Zhang, S. M. Zakeeruddin, X. Li, A. Hagfeldt, M. Grätzel, *Nat. Energy* **2016**, *1*, 16142.
- [4] W. S. Yang, B.-W. Park, E. H. Jung, N. J. Jeon, Y. C. Kim, D. U. Lee, S. S. Shin, J. Seo, E. K. Kim, J. H. Noh, *Science* **2017**, *356*, 1376–1379.
- [5] Y. Zhao, K. Zhu, *Chem. Soc. Rev.* **2016**, *45*, 655–689.
- [6] S. Akin, Y. Altintas, E. Mutlugun, S. Sonmezoglu, *Nano Energy* **2019**, *60*, 557–566.
- [7] J.-Y. Seo, H.-S. Kim, S. Akin, M. Stojanovic, E. Simon, M. Fleischer, A. Hagfeldt, S. M. Zakeeruddin, M. Grätzel, *Energy Environ. Sci.* **2018**, *11*, 2985–2992.
- [8] a) Y. Fu, T. Wu, J. Wang, J. Zhai, M. J. Shearer, Y. Zhao, R. J. Hamers, E. Kan, K. Deng, X. Y. Zhu, S. Jin, *Nano Lett.* **2017**, *17*, 4405–4414; b) K. Wojciechowski, D. Forgács, T. Rivera, *Sol. RRL*, **2019**, *3*, 1900144. doi:10.1002/solr.201900144.
- [9] T. Leijtens, G. E. Eperon, N. K. Noel, S. N. Habisreutinger, A. Petrozza, H. J. Snaith, *Adv. Energy Mater.* **2015**, *5*, 1500963.
- [10] A. J. Pearson, G. E. Eperon, P. E. Hopkinson, S. N. Habisreutinger, J. T. W. Wang, H. J. Snaith, N. C. Greenham, *Adv. Energy Mater.* **2016**, *6*, 1600014.
- [11] N. Arora, M. I. Dar, A. Hinderhofer, N. Pellet, F. Schreiber, S. M. Zakeeruddin, M. Grätzel, *Science* **2017**, *358*, 768–771.
- [12] A. Mei, X. Li, L. Liu, Z. Ku, T. Liu, Y. Rong, M. Xu, M. Hu, J. Chen, Y. Yang, M. Grätzel, H. Han, *Science* **2014**, *345*, 295–298.
- [13] B. Conings, J. Drijkoningen, N. Gauquelin, A. Babayigit, J. D'Haen, L. D'Olieslaeger, A. Ethirajan, J. Verbeeck, J. Manca, E. Mosconi, *Adv. Energy Mater.* **2015**, *5*, 1500477.
- [14] S.-H. Turren-Cruz, A. Hagfeldt, M. Saliba, *Science* **2018**, *362*, 449–453.
- [15] Y. Rong, Y. Hu, A. Mei, H. Tan, M. I. Saidaminov, S. I. Seok, M. D. McGehee, E. H. Sargent, H. Han, *Science* **2018**, *361*, eaat8235.
- [16] J. Burschka, N. Pellet, S. J. Moon, R. Humphry-Baker, P. Gao, M. K. Nazeeruddin, M. Grätzel, *Nature* **2013**, *499*, 316–319.
- [17] N. J. Jeon, J. H. Noh, W. S. Yang, Y. C. Kim, S. Ryu, J. Seo, S. I. Seok, *Nature* **2015**, *517*, 476.
- [18] M. M. Lee, J. Teuscher, T. Miyasaka, T. N. Murakami, H. J. Snaith, *Science* **2012**, *338*, 643–647.
- [19] H. S. Kim, C. R. Lee, J. H. Im, K. B. Lee, T. Moehl, A. Marchioro, S. J. Moon, R. Humphry-Baker, J. H. Yum, J. E. Moser, M. Grätzel, N. G. Park, *Sci. Rep.* **2012**, *2*, 591.
- [20] Y. Liu, S. Akin, L. Pan, R. Uchida, N. Arora, J. V. Milić, A. Hinderhofer, F. Schreiber, A. R. Uhl, S. M. Zakeeruddin, A. Hagfeldt, M. I. Dar, M. Grätzel, *Sci. Adv.* **2019**, *5*, eaaw2543.
- [21] H.-S. Kim, J.-Y. Seo, S. Akin, E. Simon, M. Fleischer, S. M. Zakeeruddin, M. Grätzel, A. Hagfeldt, *Nano Energy* **2019**, *61*, 126–131.
- [22] N. Pellet, P. Gao, G. Gregori, T.-Y. Yang, M. K. Nazeeruddin, J. Maier, M. Grätzel, *Angew. Chem. Int. Ed.* **2014**, *53*, 3151–3157; *Angew. Chem.* **2014**, *126*, 3215–3221.
- [23] W. Liao, D. Zhao, Y. Yu, N. Shrestha, K. Ghimire, C. R. Grice, C. Wang, Y. Xiao, A. J. Cimaroli, R. J. Ellingson, *J. Am. Chem. Soc.* **2016**, *138*, 12360–12363.

- [24] D. Zhao, Y. Yu, C. Wang, W. Liao, N. Shrestha, C. R. Grice, A. J. Cimaroli, L. Guan, R. J. Ellingson, K. Zhu, *Nat. Energy* **2017**, *2*, 17018.
- [25] T. Zhang, Q. Xu, F. Xu, Y. Fu, Y. Wang, Y. Yan, L. Zhang, Y. Zhao, *Sci. Bull.* **2019**, *64*, 1608–1616.
- [26] C. Yi, J. Luo, S. Meloni, A. Boziki, N. Ashari-Astani, C. Grätzel, S. M. Zakeeruddin, U. Röthlisberger, M. Grätzel, *Energy Environ. Sci.* **2016**, *9*, 656–662.
- [27] Z. Wang, Y. Zhou, S. Pang, Z. Xiao, J. Zhang, W. Chai, H. Xu, Z. Liu, N. P. Padture, G. Cui, *Chem. Mater.* **2015**, *27*, 7149–7155.
- [28] T. Niu, J. Lu, M.-C. Tang, D. Barrit, D.-M. Smilgies, Z. Yang, J. Li, Y. Fan, T. Luo, I. McCulloch, *Energy Environ. Sci.* **2018**, *11*, 3358–3366.
- [29] W. S. Yang, J. H. Noh, N. J. Jeon, Y. C. Kim, S. Ryu, J. Seo, S. I. Seok, *Science* **2015**, *348*, 1234–1237.
- [30] M. Kim, G.-H. Kim, T. K. Lee, I. W. Choi, H. W. Choi, Y. Jo, Y. J. Yoon, J. W. Kim, J. Lee, D. Huh, *Joule* **2019**, *3*(9), 2179–2192.
- [31] D. G. Billing, A. Lemmerer, *Acta Crystallogr. Sect. B* **2007**, *63*, 735–747.
- [32] M. T. Weller, O. J. Weber, J. M. Frost, A. Walsh, *J. Phys. Chem. Lett.* **2015**, *6*, 3209–3212.
- [33] P. Gratia, I. Zimmermann, P. Schouwink, J.-H. Yum, J.-N. Audinot, K. Sivula, T. Wirtz, M. K. Nazeeruddin, *ACS Energy Lett.* **2017**, *2*, 2686–2693.
- [34] C. C. Stoumpos, D. H. Cao, D. J. Clark, J. Young, J. M. Rondinelli, J. I. Jang, J. T. Hupp, M. G. Kanatzidis, *Chem. Mater.* **2016**, *28*, 2852–2867.
- [35] Y. Cho, A. M. Soufiani, J. S. Yun, J. Kim, D. S. Lee, J. Seidel, X. Deng, M. A. Green, S. Huang, A. W. Y. Ho-Baillie, *Adv. Energy Mater.* **2018**, *8*, 1703392.
- [36] H. Zhu, Y. Liu, F. T. Eickemeyer, L. Pan, D. Ren, M. A. Ruiz-Preciado, B. Carlsen, B. Yang, X. Dong, Z. Wang, H. Liu, S. Wang, S. M. Zakeeruddin, A. Hagfeldt, M. I. Dar, X. Li, M. Grätzel, *Adv. Mater.* **2020**, *32*, 1907757.
- [37] W. Q. Wu, Z. B. Yang, P. N. Rudd, Y. C. Shao, X. Z. Dai, H. T. Wei, J. J. Zhao, Y. J. Fang, Q. Wang, Y. Liu, Y. H. Deng, X. Xiao, Y. X. Feng, J. S. Huang, *Sci. Adv.* **2019**, *5*, eaav8925.
- [38] Z. P. Wang, Q. Q. Lin, F. P. Chmiel, N. Sakai, L. M. Herz, H. J. Snaith, *Nat. Energy* **2017**, *2*, 17135.
- [39] G. Grancini, C. Roldan-Carmona, I. Zimmermann, E. Mosconi, X. Lee, D. Martineau, S. Narbey, F. Oswald, F. De Angelis, M. Graetzel, M. K. Nazeeruddin, *Nat. Commun.* **2017**, *8*, 15684.
- [40] J. W. Lee, Z. H. Dai, T. H. Han, C. Choi, S. Y. Chang, S. J. Lee, N. De Marco, H. X. Zhao, P. Y. Sun, Y. Huang, Y. Yang, *Nat. Commun.* **2018**, *9*, 3021.

Manuscript received: April 13, 2020

Version of record online: June 22, 2020